11th International Congress on Engineered Material Platforms for Novel Wave Phenomena – Metamaterials 2017
Marseille, France, Aug. 28th – Sept. 2nd, 2017

Metamaterial Magnetic Resonance Imaging Endoscope

R.R.A.Syms[1], E.Kardoulaki[1], M. Rea[2], S.Taylor-Robinson[2], C.Wadsworth[2], I.R.Young[1]
[1]Imperial College London, EEE Dept., Exhibition Road, London SW7 2AZ, UK
[2]Imperial College London, Dept. of Medicine, St Mary's Hospital, Praed St., London W2 1NY, UK
r.syms@imperial.ac.uk

***Abstract* – A prototype metamaterial magnetic resonance imaging endoscope is demonstrated, based on flexible, non-magnetic components and a thin-film magneto-inductive receiver. The receiver can form an image along the entire insertion tube and phantom experiments show a signal-to-noise-ratio advantage over a surface array coil to 3 times the tube diameter at the tip.**

I. Introduction

In well-designed receivers, the signal-to-noise ratio (SNR) obtained in magnetic resonance imaging (MRI) of human subjects is limited by noise from the body itself, rather than the detection coil [1]. Consequently, increased SNR and image resolution can be obtained using coils with restricted fields of view (FOV), provided these encompass the target tissue. There has been sustained interest in the development of small internal coils for imaging of lumens such as arteries, ducts and the GI tract. For compatibility with clinical procedures these are normally based on endoscopes [2], [3] or catheters [4], [5]. Some metamaterial internal imaging systems (the wire medium endoscope [6], and the magneto-inductive (MI) catheter [7]) have already been proposed. The latter has the advantage that its segmented construction has no extended linear conductors (which may be excited into resonance by external electric fields) and consequently provides intrinsic safety. Here we demonstrate an early prototype MR-imaging endoscope based on the same principle and operating at 3T.

II. Design

In contrast to earlier MR-imaging endoscopes, which provide an image only near a tip-mounted coil, the new instrument is designed to image the GI tract from the esophagus to the duodenum. To achieve this, a receiver with a concentric cylindrical FOV is mounted along the entire length of the insertion tube, as shown in Fig. 1a. Because the tube is crowded with a disc stack and channels for steering cables, optics and biopsy, the receiver is a flexible thin-film circuit intended for mounting between the inner and outer sheath as shown in Fig. 1b.

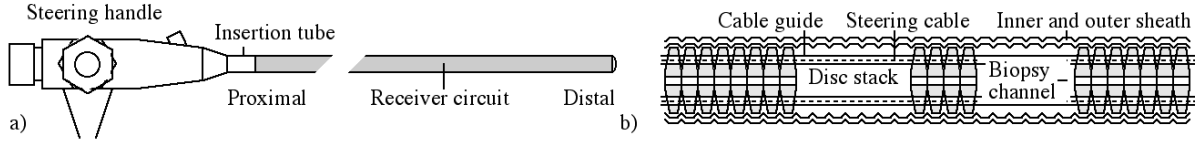

Fig. 1. a) MR-imaging endoscope, and b) detail of insertion tube.

Fig. 2a shows the equivalent circuit, which is based on a self-terminating MI system. The main section consists of a uniform MI waveguide [8], formed from a cascade of L-C resonators (with resistance R), coupled to their neighbours by a mutual inductance M. Each element resonates at angular frequency $\omega_0 = 1/\sqrt{(LC)}$ and the waveguide has a characteristic impedance $Z_{0M} = \omega_0 M$ at resonance. At the distal end, the waveguide is terminated using a similar element, and matched self-termination is achieved using a mutual inductance M' such that $\omega_0 M' = \sqrt{(Z_0 R)}$. At the proximal end, the waveguide is connected to a broadband coupling transducer based on a halved element with inductance L/2 and capacitance 2C (and hence the same resonant frequency). Matching to the scanner impedance Z_0 is achieved using a mutual inductance M" such that $\omega_0 M'' = \sqrt{(Z_0 Z_{0M})}$.

Fig. 2b shows the circuit layout. Each element is constructed from a printed inductor and a pair of parallel plate capacitors that use the substrate as an interlayer dielectric. To prevent coupling to the B_1 field during the excitation phase of MRI, the inductors are figure-of-eight shaped. Similarly, to prevent coupling to the E field

ISBN 978-88-941141-2-6

[9], the length of each element is less than the minimum length for excitation of a half-wave standing wave resonance of an immersed wire. These two features effectively make the circuit invisible during excitation.

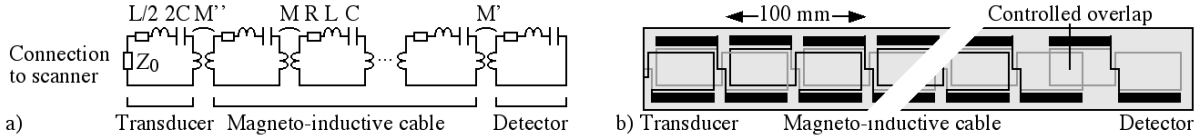

Fig. 2. a) Equivalent circuit and b) thin-film realization of magneto-inductive receiver.

Electrical response was simulated by solving the loop equations for the circuit model in Fig. 2a, with the resonant frequency chosen to match the Larmor frequency for protons in a 3T magnetic field (127.7 MHz). The circuit was assumed to act as a transmitter, with a signal derived from the scanner itself and an inductive probe connected to a load Z_0 to detect the signal at the tip. Fig. 3a shows the response obtained, for a circuit based on a 19 element MI waveguide with parameters L = 270 nH, R = 2.5 Ω, C = 5.8 pF, and M = 83.5 nH, chosen for comparison with experimental values. These parameters correspond to a Q-factor $\omega_0 L/R = 85$, a coupling coefficient $\kappa = 2M/L = 0.62$ and a characteristic impedance $Z_{0M} = 67$ Ω. The response is clearly that of a resonant detector, peaking sharply at the design frequency and with good corresponding matching.

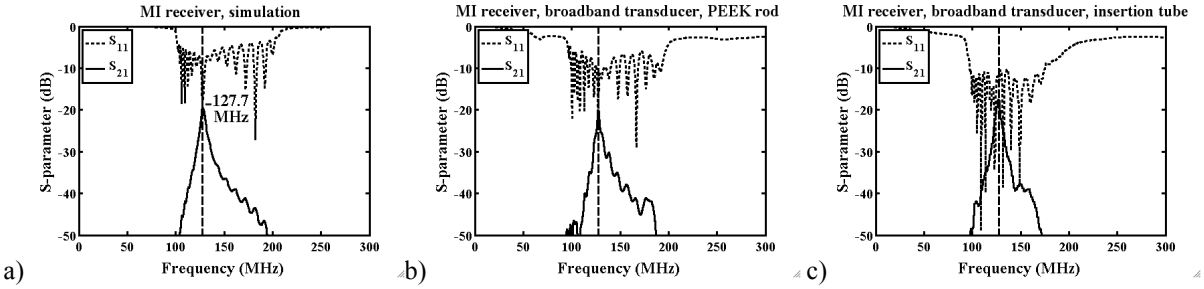

Fig. 3. Receiver responses: a) theoretical, b) experimental, on PEEK scaffold, c) experimental, on insertion tube.

III. Construction and Electrical Testing

Thin-film circuits were fabricated by the UK company Clarydon by double-sided patterning and etching of 1 m long copper-clad Kapton® HN sheets (37.5 µm Cu + 25 µm polyimide; Dupont) with the CAD layout in Fig. 4a, following the established method of forming MI cables [10]. Track widths of 0.5 mm and 0.75 mm were used for inductors and capacitors, respectively. Element widths (41 mm) were designed for mounting on a 13 mm diameter tube, while element lengths (100 mm) were made less than that of a λ/2 dipole (≈ 130 mm at 127.7 MHz) in tissue, a medium of relative dielectric constant $\varepsilon_r \approx 77$ at radio frequency. Circuits were formed as 19-element cables with separate transducers and final elements. Additional test elements were also provided.

Electrical testing was carried out using a network analyzer. The parameter values above were extracted by inductively probing single and paired elements with printed capacitors and with capacitors of known value. Circuits were mounted on a cylindrical PEEK rod, and the capacitors were trimmed to set the resonant frequency. The position of the terminating element was established by observing Q-factor halving using an inductive pickup. Fig. 3b shows the frequency response of the final circuit, in good agreement with Fig. 3a.

Fig. 4. a) CAD layout of PCBs; b) flexible insertion tube; c) PCB after frequency tuning, cutout and mounting.

Non-magnetic insertion tubes with the design of Fig. 1b and a diameter of 13 mm were fabricated by the UK

company Endoscan, as shown in Fig. 4b. To improve RF compatibility, metal spirals normally used to guide the Dyneema® steering cables were replaced with PTFE tubing. Similarly, to enhance mechanical flexibility, excess Kapton was removed from the thin-film circuit, which was attached to the insertion tube as shown in Fig. 4c. A reduction in Q-factor from 85 to 50 was then observed, ascribed to dielectric loss in the outer polyurethane sheath. Despite this, the frequency response was similar, as shown in Fig. 3c.

IV. Magnetic Resonance Imaging

Imaging was carried out using a GE MR750 Discovery scanner. The MI endoscope was arranged in an S-shaped path parallel to the magnet bore between two cuboid phantoms filled with tissue-mimicking fluid as shown in Fig. 5a. The body coil was used for excitation, and an 8-element array coil for comparison. Localiser and array images showed little perturbation to the magnetisation, suggesting effective decoupling. Imaging was carried out with a spin-echo sequence with a 90° flip angle, TE = 10 ms, TR = 500 ms and a 5 mm slice thickness. Fig. 5b shows a sagittal image at the edge of one cuboid obtained using the metamaterial endoscope, which shows segmented image formation following the track of the insertion tube. Fig. 5c shows an axial image, which has high SNR adjacent to the tube but highlights the restricted FOV. Fig. 5d compares the radial variation of SNR at three positions with a variation obtained using the array coil. At its tip, the metamaterial endoscope provides higher SNR to a diameter of 45 mm, more than three times the tube diameter, confirming localised SNR gain.

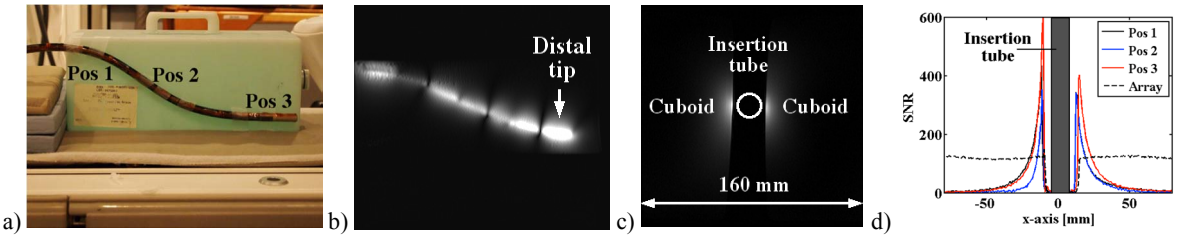

Fig. 5. a) Arrangement for MRI, b), c) sagittal and axial images, and d) comparative radial variation of SNR.

V. Conclusions

A prototype MRI endoscope capable of imaging along the length of its insertion tube has been demonstrated, by combining non-magnetic components with a thin film magneto-inductive receiver. Phantom experiments show a SNR gain compared with a chest coil array to over three times the diameter of the insertion tube.

References

[1] D.I. Hoult and P.C. Lauterbur, "The sensitivity of the zeugmatographic experiment involving human samples," *J. Magn. Reson.*, vol. 34, p. 425-433, 1979.
[2] K. Inui, S. Nakazawa, J. Yoshino et al., "Endoscopic MRI: preliminary results of a new technique for visualization and staging of gastrointestinal tumors," *Endoscopy*, vol. 27, p. 480-485, 1995.
[3] D.J. Gilderdale, A.D. Williams, U. Dave and N.M. deSouza, "An inductively-coupled, detachable receiver coil system for use with magnetic resonance compatible endoscopes," *JMRI*, vol. 18, p. 131-135, 2003.
[4] H.L. Kantor, R.W. Briggs and R.S. Balaban, "In vivo ^{31}P nuclear magnetic resonance measurements in canine heart using a catheter-coil," *Circ. Res.*, vol. 55, p. 261-266, 1984.
[5] P.A. Bottomley, E. Atalar, R.F. Lee, K.A. Shunk and A. Lardo, "Cardiovascular MRI probes for the outside in and for the inside out," *Magn. Res. Mats. Phys., Biol. Med.*, vol. 11, p. 49-51, 2000.
[6] X. Radu, D. Garray and C. Craeye, "Towards a wire medium endoscope for MRI imaging," *Metamaterials*, vol. 3, 90-99, 2009.
[7] R.R.A. Syms, I.R. Young, M.M. Ahmad, S.D. Taylor-Robinson and M. Rea, "Magneto-inductive catheter receiver for magnetic resonance imaging," *IEEE Trans. Biomed. Engng.*, vol. 60, p. 2421-2431, 2013.
[8] E. Shamonina, V.A. Kalinin, K.H. Ringhofer and L. Solymar, "Magneto-inductive waveguide," *Elect. Lett.*, vol. 38, p. 371-373, 2002.
[9] M.K. Konings, L.W. Bartels, H.F.M. Smits and C.J.G. Bakker, "Heating around intravascular guidewires by resonating RF waves," *JMRI*, vol. 12, p. 79-95, 2000.
[10] R.R.A. Syms, I.R. Young, L. Solymar and T. Floume, "Thin-film magneto-inductive cables," *J. Phys. D. Appl. Phys.*, vol. 43, 055102, 2010.

ISBN 978-88-941141-2-6